The Calculated and Measured Temperature Distribution of a Phased Interstitial Antenna Array

YANG ZHANG, WILLIAM T. JOINES, MEMBER, IEEE, AND JAMES R. OLESON

Abstract—**The power deposition pattern of four antennas, positioned on the corners of a 2 cm square array with different driving phases, is computed under the assumption of negligible coupling between the antennas. The spatial *SAR* (specific absorption rate) distribution is calculated by modeling each interstitial applicator as an insulated, asymmetric dipole. For comparison with the heating patterns measured by a thermal video system, the calculated *SAR* distributions are converted into temperature patterns through an electric network simulation of the heating in artificial muscle tissue. At each nodal point of a grid in the thermal system, the absorbed microwave power (or *SAR* times density), thermal resistivity, heat capacitance, and temperature are simulated, respectively, as current source, electrical resistance, electrical capacitance, and potential. Therefore, solving the equivalent electric network on a computerized simulation routine (SPICE) yields the temperature distribution. In both the axial and transverse planes, the resulting temperature distributions from the antenna array, with various driving phases, agree very well with the measured temperature patterns.**

I. INTRODUCTION

THERE CONTINUES to be a high level of interest in the application of microwave-induced hyperthermia in the treatment of cancer. Although noninvasive techniques are usually preferred in clinical treatments, there are disadvantages and difficulties in controlling the heating patterns of the noninvasive microwave applicators [1], [2]. Invasive applicators (or interstitial antennas), inserted directly into the tissue region to be heated, often result in better control of the heating pattern, both within and outside the target region. The possibility of using interstitial microwave antennas inserted directly into the tumor was first suggested by Mendecki *et al.* [3] and Taylor [4] in 1977 and 1978. These coaxial line antennas are usually about 1 mm in diameter, have a radiating gap (or gaps) in the outer conductor, and are inserted into a plastic catheter that is embedded in the region to be heated [5], [6]. A single interstitial antenna (radiating at 915 MHz) will heat a tissue volume of about 5 cm along the axis of the antenna and about 2 cm in diameter transverse to the antenna [7]. The limited heating volume generated by a single antenna is often unsatisfactory because most tumors seen in the clinic are more than 2 cm in diameter. Therefore, it is necessary to use an array of two or more microwave antennas in order to heat the entire tumor volume.

A number of researchers have investigated applications using interstitial antenna arrays. Most of the published results are based upon experiments [8]–[12]. Recently, King *et al.* [13] proposed a symmetric dipole model to simulate the interstitial antenna, from which the electric field distribution surrounding the antenna was determined. In subsequent studies, Trembly *et al.* applied the symmetric dipole model to calculate the power deposition pattern with an interstitial antenna array [14]–[16]. They demonstrated that changing the driving frequency, phase, and antenna length does in fact alter the *SAR* (specific absorption rate) pattern within the array. Zhang *et al.* [17] proposed an asymmetric dipole model for the interstitial applicators. It was found that this model yields close agreement between calculated and measured *SAR* distributions for a number of interstitial antennas having different dimensions.

The present study is a continuation of the work presented in [17]. The asymmetric insulated dipole is used to simulate each antenna in the array. The object of this investigation is to determine and compare the theoretical and measured heating patterns produced by an array of four antennas positioned on the corners of 2 cm square. Each antenna is driven with equal power at 915 MHz, but with various relative phase angles. The actual heating patterns produced by the array are measured using a thermal graphic camera. In order to compare relevant parameters, the calculated *SAR* distributions are converted into temperature patterns through an electric network simulation of the heat flow [18], [19]. The antenna-generated power deposition at points in the thermal system becomes current-source inputs at nodal points of the electrical system. Therefore, solving the equivalent electric network on a computerized simulation routine yields the temperature distribution. It was found that in both the axial and lateral planes, the resulting theoretical temperature distributions from the antenna array, with various

Manuscript received December 6, 1988; revised August 23, 1989. This work was supported by PHS under Grant 1 pol CA42745-01A1, awarded by the National Cancer Institute, DHHS.

Y. Zhang and W. T. Joines are with the Department of Electrical Engineering, Duke University, Durham, NC 27706.

J. R. Oleson is with the Division of Radiation Oncology, Duke University Medical Center, Durham, NC 27710.

IEEE Log Number 8931775.

0018-9480/90/0100-0069$01.00

driving phases, agree very well with the measured temperature patterns.

II. Theory of Phased Antenna Array

An interstitial antenna with catheter, embedded in biological tissue, can be simulated as an asymmetric dipole when certain conditions are satisfied [17]. Specifically, when a linear, insulated antenna in an electrically dense medium is electrically thin (length-to-diameter and wavelength-to-diameter ratios greater than about 15 [20]) and when the medium permittivity is much greater than the insulator permittivity, then the structure may be treated with good accuracy as a section of suitably terminated coaxial transmission line [21], [22]. Under these conditions the current distribution on the antenna has a relatively simple form, from which the electric field expressions at points around the antenna are derived. Since a detailed discussion is presented in [17] for a single antenna, only the expressions to be used in the electric field calculations of the antenna array are listed here.

The structure of an insulated asymmetric dipole antenna, its dimensions, and the associated coordinates are illustrated in Fig. 1. The antenna consists of two central conductors (region 1), of length h_1 and h_2 and radius a, surrounded by a cylinder of dielectric consisting of one or two layers (regions 2 and 3), respectively, of outer radii b and c. Region 4 is the surrounding ambient medium, or tissue. This region is assumed to be homogeneous and infinite in extent. The wavenumbers of the insulating layers and the ambient medium are given, respectively, by $k_2 = \omega(\mu_0\epsilon_2)^{1/2}$, $k_3 = \omega(\mu_0\epsilon_3)^{1/2}$, and $k_4 = \beta_4 + j\alpha_4 = \omega(\mu_0\tilde{\epsilon}_4)^{1/2}$, where $\tilde{\epsilon}_4 = \epsilon_4 + j\sigma_4/\omega$, μ_0 is the permeability of free space, ω is the radian frequency, ϵ_i $(i = 2,3,4)$ are the dielectric constants of each region, and σ_4 is the conductivity of tissue. A time dependence of $e^{j\omega t}$ is assumed for all fields. If the following conditions:

$$|k_4/k_2|^2 \gg 1 \qquad |k_4/k_3|^2 \gg 1$$
$$(k_2 b)^2 \ll 1 \qquad (k_3 c)^2 \ll 1 \tag{1}$$

are satisfied, the electric field components in the ambient medium produced by the antenna are given by [17]

$$\begin{aligned} E_{4z}(r,z) = {} & \frac{I_0}{4\pi^2 \sin k_L h_1}\left\{ j\omega\mu_0 \int_0^{h_1}\int_0^{\pi} \sin k_L(h_1 - z')\frac{e^{jk_4R}}{R}\,d\phi'\,dz' \right. \\ & + j\omega\mu_0 c \ln\left(\frac{c}{a}\right)\left(1 - \frac{k_L^2}{k_{2e}^2}\right)\int_0^{h_1}\int_0^{\pi} \sin k_L(h_1 - z')\frac{e^{jk_4R}}{R^2}\left(\frac{1}{R} - jk_4\right)(c - r\cos\phi')\,d\phi'\,dz' \\ & \left. + \frac{jk_L}{\tilde{\epsilon}_4\omega}\int_0^{h_1}\int_0^{\pi}(z - z')\cos k_L(h_1 - z')\frac{e^{jk_4R}}{R^2}\left(\frac{1}{R} - jk_4\right)d\phi'\,dz' \right\} \\ & + \frac{I_0}{4\pi^2 \sin k_L h_2}\left\{ j\omega\mu_0 \int_{-h_2}^{0}\int_0^{\pi} \sin k_L(h_2 + z')\frac{e^{jk_4R}}{R}\,d\phi'\,dz' \right. \\ & + j\omega\mu_0 c \ln\left(\frac{c}{a}\right)\left(1 - \frac{k_L^2}{k_{2e}^2}\right)\int_{-h_2}^{0}\int_0^{\pi} \sin k_L(h_2 + z')\frac{e^{jk_4R}}{R^2}\left(\frac{1}{R} - jk_4\right)(c - r\cos\phi')\,d\phi'\,dz' \\ & \left. - \frac{jk_L}{\tilde{\epsilon}_4\omega}\int_{-h_2}^{0}\int_0^{\pi}(z - z')\cos k_L(h_2 + z')\frac{e^{jk_4R}}{R^2}\left(\frac{1}{R} - jk_4\right)d\phi'\,dz' \right\} \end{aligned} \tag{2}$$

and

$$\begin{aligned} E_{4r}(r,z) = {} & \frac{I_0}{4\pi^2 \sin k_L h_1}\left\{ j\omega\mu_0 c \ln\left(\frac{c}{a}\right)\left(1 - \frac{k_L^2}{k_{2e}^2}\right) \right. \\ & \cdot \int_0^{h_1}\int_0^{\pi} \sin k_L(h_1 - z')\frac{e^{jk_4R}}{R^2}\left(\frac{1}{R} - jk_4\right)(z - z')\cos\phi'\,d\phi'\,dz' \\ & \left. - \frac{jk_L}{\tilde{\epsilon}_4\omega}\int_0^{h_1}\int_0^{\pi} \cos k_L(h_1 - z')\frac{e^{jk_4R}}{R^2}\left(\frac{1}{R} - jk_4\right)(c\cos\phi' - r)\,d\phi'\,dz' \right\} \\ & + \frac{I_0}{4\pi^2 \sin k_L h_2}\left\{ j\omega\mu_0 c \ln\left(\frac{c}{a}\right)\left(1 - \frac{k_L^2}{k_{2e}^2}\right) \right. \\ & \cdot \int_{-h_2}^{0}\int_0^{\pi} \sin k_L(h_2 + z')\frac{e^{jk_4R}}{R^2}\left(\frac{1}{R} - jk_4\right)(z - z')\cos\phi'\,d\phi'\,dz' \\ & \left. + \frac{jk_L}{\tilde{\epsilon}_4\omega}\int_{-h_2}^{0}\int_0^{\pi} \cos k_L(h_2 + z')\frac{e^{jk_4R}}{R^2}\left(\frac{1}{R} - jk_4\right)(c\cos\phi' - r)\,d\phi'\,dz' \right\} \end{aligned} \tag{3}$$

where

$$I_0 = V_0^e / Z_A \tag{4}$$

$$Z_A = \frac{Z_1 + Z_2}{2} \tag{5}$$

$$Z_1 = j\frac{2Z_c}{\tan k_L h_1} \tag{6}$$

$$Z_2 = j\frac{2Z_c}{\tan k_L h_2} \tag{7}$$

$$k_L = k_{2e}\left[\frac{\ln(c/a) + F}{\ln(b/a) + n_{24}^2 F}\right]^{1/2} \tag{8}$$

$$F = \frac{H_0^{(1)}(k_4 c)}{k_4 c H_1^{(1)}(k_4 c)} \tag{9}$$

$$k_{2e} = k_2\left[\frac{\ln(c/a)}{\ln(b/a) + n_{23}^2 \ln(c/b)}\right]^{1/2} \tag{10}$$

$$\epsilon_{2e} = \epsilon_2 \frac{\ln(c/a)}{\ln(b/a) + n_{23}^2 \ln(c/b)} \tag{11}$$

$$n_{2e4}^2 = k_{2e}^2 / k_4^2 \tag{12}$$

$$n_{23}^2 = k_2^2 / k_3^2 \tag{13}$$

$$n_{24}^2 = k_2^2 / k_4^2 \tag{14}$$

$$Z_c = \frac{\omega \mu_0 k_L}{2\pi k_{2e}^2}\left[\ln(c/a) + n_{2e4}^2 F\right] \tag{15}$$

$$R = \left[(z - z')^2 + (r - r')^2 + 4rr' \sin^2 \frac{\phi'}{2}\right]^{1/2}\Bigg|_{r'=c}. \tag{16}$$

$H_0^{(1)}(x)$ and $H_1^{(1)}(x)$ are Hankel functions, and V_0^e is the voltage at the input junction. Z_A is the input impedance. Note that regions 2 and 3 have been combined as one effective region of permittivity ϵ_{2e} and wavenumber k_{2e}. Equations (2) and (3) may be evaluated numerically using the Gaussian quadrature formula [17], [23] and the adaptive Simpson rule [24], [25].

Once the electric field is known for a single antenna, the total electric field at any point in the array may be computed by summing up the contributions from each antenna with the phase angles taken into account. Fig. 2 shows the structure of the four-antenna array and the definitions of the coordinates. The antennas are placed with their axes in parallel and with the radiation gaps at the aligned junction plane $z = 0$. It is assumed that the output of one antenna is not altered by the presence of the other three, or the effect of coupling between the antennas may be neglected. In fact, theoretical calculations indicate that at 2 cm from a radiating gap in muscle tissue the *SAR* is diminished by at least a factor of 4 below the *SAR* produced at the gap. Therefore, ignoring the coupling between the antennas seems reasonable. The electric field

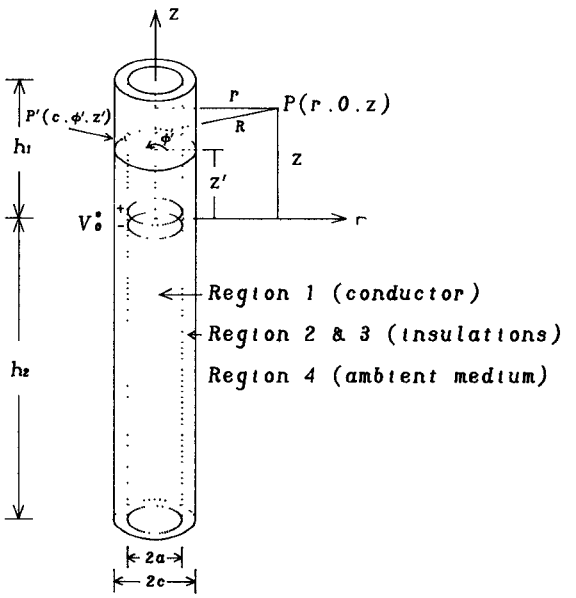

Fig. 1. Insulated asymmetric dipole in ambient medium. The antenna is fed from the bottom through a coaxial cable. The relevant dimensions are $h_1 = 1.989$ cm, $h_2 = 13$ cm, $a = 0.475$ mm, and $c = 0.805$ mm.

components at a point (x, y, z) in space are determined by

$$E_x = \frac{x-a}{R_1}E_{r1}e^{j\theta_1} + \frac{x+a}{R_2}E_{r2}e^{j\theta_2} + \frac{x+a}{R_3}E_{r3}e^{j\theta_3} + \frac{x-a}{R_4}E_{r4}e^{j\theta_4} \tag{17}$$

$$E_y = \frac{y-a}{R_1}E_{r1}e^{j\theta_1} + \frac{y-a}{R_2}E_{r2}e^{j\theta_2} + \frac{y+a}{R_3}E_{r3}e^{j\theta_3} + \frac{y+a}{R_4}E_{r4}e^{j\theta_4} \tag{18}$$

and

$$E_z = E_{z1}e^{j\theta_1} + E_{z2}e^{j\theta_2} + E_{z3}e^{j\theta_3} + E_{z4}e^{j\theta_4} \tag{19}$$

where θ_i $(i = 1, \cdots, 4)$ are the phase angles of the antennas, and

$$R_1 = \sqrt{(x-a)^2 + (y-a)^2} \tag{20}$$

$$R_2 = \sqrt{(x+a)^2 + (y-a)^2} \tag{21}$$

$$R_3 = \sqrt{(x+a)^2 + (y+a)^2} \tag{22}$$

and

$$R_4 = \sqrt{(x-a)^2 + (y+a)^2}. \tag{23}$$

We have assumed that the junctions of antennas 1–4 are located at $(a, a, 0)$, $(-a, a, 0)$, $(-a, -a, 0)$, and $(a, -a, 0)$, respectively. E_{ri} and E_{zi} $(i = 1, \cdots, 4)$ are computed, respectively, by (2) and (3) for each antenna. The distance a is set to 1 cm for this study.

The power absorbed per unit mass (*SAR*) signifies the rate of heat generation and is given by

$$SAR = \frac{\sigma_4}{2\rho}\left(|E_x|^2 + |E_y|^2 + |E_z|^2\right) \tag{24}$$

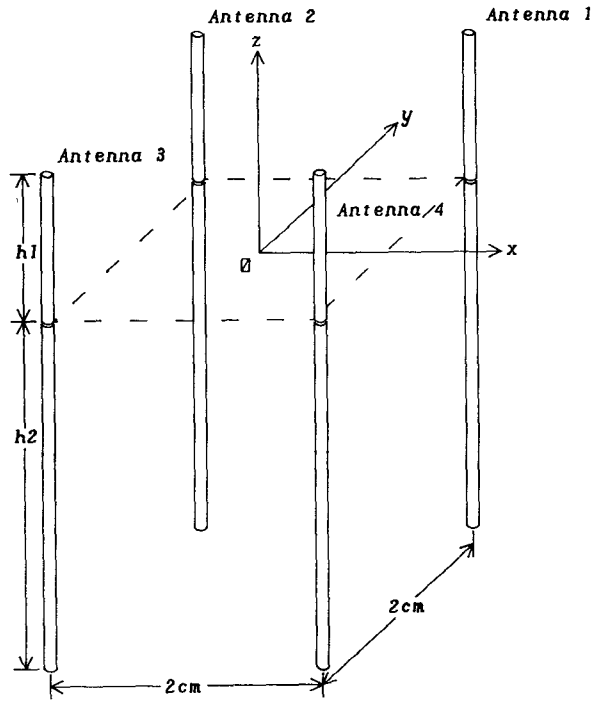

Fig. 2. Square array of interstitial antennas. Detail of each antenna is shown in Fig. 1.

where σ_4 is the electrical conductivity of the biological tissue, and ρ is the density of the medium. Equation (24) gives the spatial *SAR* distribution within the array as a function of position relative to the antennas. It is this quantity that is of interest in microwave-induced hyperthermia applications.

III. Derivation of Temperature Distribution from *SAR* Pattern

To directly compare the theoretical predictions of *SAR* patterns with experiment, the *SAR* profiles of the antenna array would have to be measured. To do this for the antenna array, the temperature history in real time would have to be measured at all points in the 3-D space [7]. A more practical alternative is to measure the temperature profiles on a particular plane using a thermal graphic camera. The theoretical *SAR* patterns are then converted into temperature profiles through a numerical simulation of heat conduction. Thus, a comparison between theory and measurement is in fact accomplished.

To convert *SAR* to temperature, an electrical analogy to heat flow within phantom muscle tissue is presented [18], [19]. With this technique, the physical region of interest is partitioned into a system of finite sections or blocks, as shown in Fig. 3(a). The mass of each block is represented by a point or node in the center of the block. The paths for the transfer of heat from one block to another are represented by heat conductors connecting the nodes. If, as in Fig. 3(b), the dimensions of each block are Δx, Δy, and Δz, respectively, along the x, y, and z directions, the heat

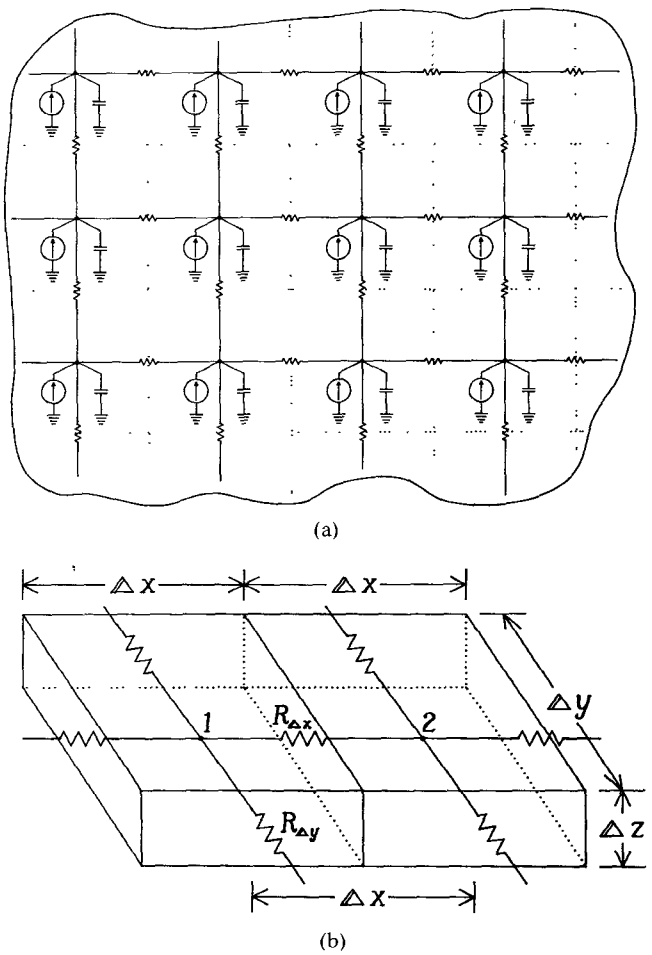

Fig. 3. (a) Electric network analogy to heat flow. The region is divided into blocks. (b) Two typical blocks.

resistances (in °C/W) in each direction are obtained by

$$R_x = \frac{1}{k}\frac{\Delta x}{\Delta y \Delta z} \tag{25}$$

$$R_y = \frac{1}{k}\frac{\Delta y}{\Delta x \Delta z} \tag{26}$$

$$R_z = \frac{1}{k}\frac{\Delta z}{\Delta x \Delta y} \tag{27}$$

where k (in W/m°C) is the thermal conductivity of the material, or tissue. Attached to each node is a thermal capacitor controlling the temperature response of the node to a given quantity of heat. The value of this capacitor is the amount of heat necessary to raise the temperature of the mass in the block 1°C and is given by

$$C_t = \rho c_p \Delta V = \rho c_p \Delta x \Delta y \Delta z \tag{28}$$

where C_t is in J/°C and c_p is the specific heat in J/kg°C. ΔV is the volume of the block. The microwave power absorbed in each block is signified by a heat flux source injected into the node. This quantity is determined by the *SAR* at the nodal point as

$$I = SAR\rho\Delta V = SAR\rho\Delta x \Delta y \Delta z \tag{29}$$

where the heat flux I is in W if SAR is in W/kg and ρ is in kg/m^3.

In our experiments, phantom muscle tissue is used as the irradiated medium [26]. Therefore, no blood flow is considered, and the medium is homogeneous. The effect of blood flow could easily be incorporated by adding convective elements to the nodes [19], and an inhomogeneous medium could be simulated by using differing values of heat resistances and capacitances. In this study, the ambient temperature is enforced on a boundary that is 3 cm away from the array. This distance was chosen by running several simulations and varying the boundary until the temperature distribution in the array became insensitive (temperature change less than 1 percent) to the location of the boundary.

If the heat flux, thermal resistance, heat capacitance, and temperature in the thermal system are simulated, respectively, as current source, electrical resistance, electrical capacitance, and potential, an equivalent electric network is achieved. Solving the electric network and plotting the transient electric potential distribution yield the temperature profile for the thermal system. It should be noted that solving the transient response of the system is necessary since the measurement of temperature in the array is made before steady-state conditions are reached. A computerized network simulation routine, SPICE [27], is used to solve the transient response of the electric network. This computer program allows one to solve a system many orders of magnitude larger than the one we have considered (we used 1161 nodes, with 2389 resistors, 1160 capacitors, and 756 current sources for the simulations in the $x-z$ plane). The practical limitation one first encounters is the computer memory space.

IV. Theoretical and Experimental Results

Four interstitial antennas were constructed from semi-rigid microwave coaxial cable (Micro-coax, UT-34M), which has an outer radius $a = 0.475$ mm. The tip length (h_1 in Fig. 1) was 1.989 cm, and h_2 was 13.0 cm. The determination of h_2 has been discussed in [17]. A quarter-wavelength stripline matching circuit was constructed for each of the antennas, so that the measured input return loss was greater than 20 dB. The insulating dielectric in Fig. 1 has two layers. The inner layer of air between the antenna and the catheter has an outer radius $b = 0.584$ mm and a relative permittivity $\epsilon_{2r} = 1$. The outer layer of insulation is the catheter (polypropylene catheter, 5FR., Monoject, Division of Sherwood Medical) of outer radius $c = 0.805$ mm and relative permittivity $\epsilon_{3r} = 2.55$ [28]. The ambient medium is phantom muscle tissue [26] of relative permittivity $\epsilon_{4r} = 51$, conductivity $\sigma_4 = 1.28$ S/m, and density $\rho = 970$ kg/m^3. The antennas are operated at 915 MHz with V_0^e set to 1 V. This assumed value of V_0^e will not affect the results since the calculated temperature distributions are normalized to make the comparison with experiments meaningful. Note that the conditions in (1) are well satisfied by this system.

Calculations and measurements are accomplished on two major planes: the lateral plane through $z = 0$ and the axial plane through $y = 0$, for various combinations of phase angles. Because of the limitation on the length of the paper, only two phase combinations are presented. The theoretical iso-SAR distributions generated using (24) are illustrated, respectively, in (a) and (b) of Fig. 4. The SAR values have been normalized to their maximum values and are plotted as percentile contours. Parts (a) and (b) in Fig. 4 show the iso-SAR patterns in the planes through $z = 0$ and $y = 0$, respectively, for an array in which all four antennas are in phase.

The SAR distributions in (a) and (b) of Fig. 4 are converted into temperature patterns, represented by the contour lines in parts (c) and (d) of the same figure, using the procedures described in the previous section. The specific heat of phantom muscle tissue is $c_p = 3{,}516$ J/kg°C with thermal conductivity $k = 0.544$ W/m°C [29]. A two-dimensional model is used in the analysis because of the limitation on the computer memory space. In the lateral plane ($z = 0$), the grid size is 2 mm (Δx) by 2 mm (Δy), whereas 2 mm (Δx) by 4 mm (Δz) grids are used in the axial plane ($y = 0$). The SAR calculations in the array are computed with the same grid sizes. The nodal temperature values are obtained after a simulated microwave heating time of 6 minutes (also the experimental heating time). The temperature increments obtained by subtracting the initial temperature (25°C) from the final temperature are then normalized to the maximum value. The results obtained for axial and lateral planes are illustrated, respectively, in (c) and (d) of Fig. 4. Fig. 5 shows the temperature patterns generated by the array with different phase inputs. In this case, antennas 1 and 4 are in phase at 180°, and antennas 2 and 3 are in phase at 0°. The corresponding SAR patterns are not shown.

The temperature measurements are performed on phantom muscle tissue [26] in two boxes (10 cm × 10 cm × 18 cm) made from polystyrene sheets. One box is divided into two parts along the lateral plane, and the other along the axial plane. This setup allows a fast access to the planes of interest in the phantom muscle tissue for making temperature measurements. With one of the boxes, the temperature distribution in the lateral plane at $z = 0$ is measured on an area of 10 cm by 10 cm. With the other box of phantom tissue, the temperature pattern in the axial plane at $y = 0$ is recorded on an area of 10 cm by 18 cm. The four interstitial antennas are driven by the same microwave source (model 15022, MCL Inc.). A power divider separates the signal into four equal and in-phase parts. Two continuously adjustable delay lines (trombone sections) are used to vary the phase angles. A thermal video system (Probeye, model 3300, Hughes Aircraft Company) is used to record the temperature patterns after the phantom tissue is irradiated for 6 minutes at an input power of 5 W to each antenna. These recorded patterns on the lateral and axial planes are photographed, and then transferred onto the theoretical temperature plots in Figs. 4 and 5,

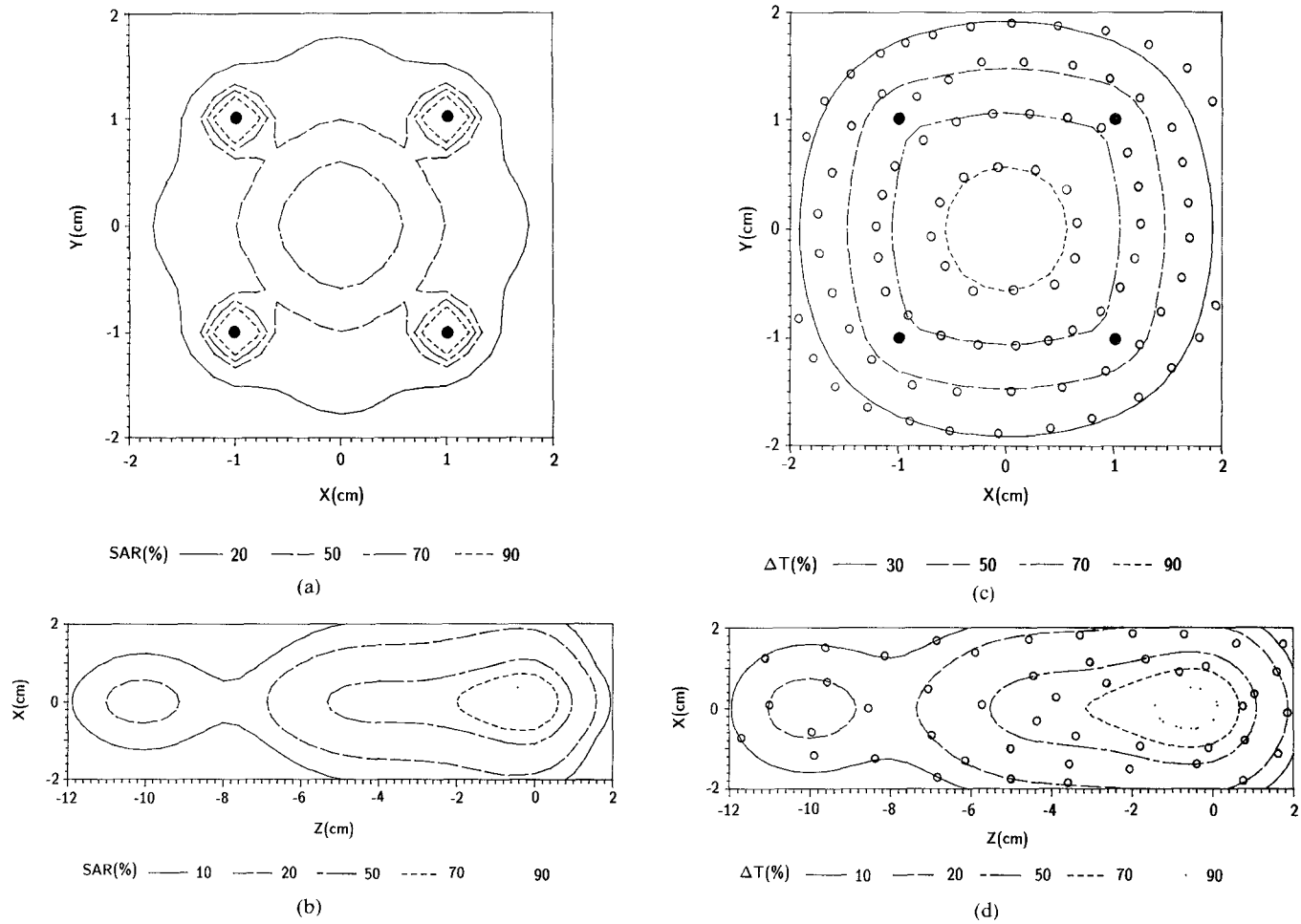

Fig. 4. Calculated and measured results for an in-phase antenna array. (a) Calculated *SAR* distribution in the plane $z = 0$. The *SAR* values are normalized to their maximum. Labels refer to the iso-*SAR* levels in percentage. The black dots show the antenna positions. (b) Same as (a), but in the plane $y = 0$. The antenna gaps are at $z = 0$. (c) Theoretical (various contour lines) and measured (open circles) temperature pattern in the plane $z = 0$. The temperature increments are normalized to their maximum. Labels refer to the normalized isotemperature increment levels in percentage. The antenna positions are shown as black dots. (d) Same as (c), but in the plane $y = 0$.

respectively, for the two cases of different phase combinations. The measured patterns are represented as open circles in Figs. 4 and 5.

V. Discussion

In microwave-induced hyperthermia applications, the value of *SAR* is directly proportional to the rate of temperature increase when the rate of increase greatly exceeds the rates of decrease due to heat conduction and blood perfusion. A steep gradient in *SAR* may not correspond to a steep temperature gradient, because of the smoothing effects of heat conduction (and blood perfusion in live tissue). For example, refer to Fig. 4, where the calculated *SAR* and temperature patterns, along with the measured temperature profiles, are illustrated, respectively, in the two planes at $z = 0$ and at $y = 0$ for an in-phase array. In parts (a) and (c) of Fig. 4, the predicted *SAR* and temperature patterns in the lateral plane ($z = 0$) have their maximum value in the center of the array. The *SAR* varies by only 50 percent over the entire region between the antennas. Although there exist steep gradients in *SAR* near each antenna, the temperature distribution is quite smooth due to heat conduction. The isotemperature contours of 65 percent and above include the entire region of the array. Also shown on Fig. 4(c) are the measured heating patterns represented by the open circles. The agreement between theory and experiment is very good at the higher temperature elevations, but not as good at the lower elevations. This is because the noise in our measurement system makes the lower temperature (closer to ambient) more difficult to resolve.

The calculated *SAR*, temperature, and measured temperature profiles in the axial plane ($y = 0$) are presented in Fig. 4(b) and (d) respectively. The theoretical results of both *SAR* and temperature show that heating above 50 percent occurs over a region 2 cm by 6 cm. The measured temperature profiles in Fig. 4(d) cover about the same region for 50 percent heating and thus agree quite well with the computed temperature profiles (Fig. 4(d)). There is a secondary peak at about $z = -10$ cm in both the calculated and the measured results. In both cases, this secondary peak is small enough to be ignored in most

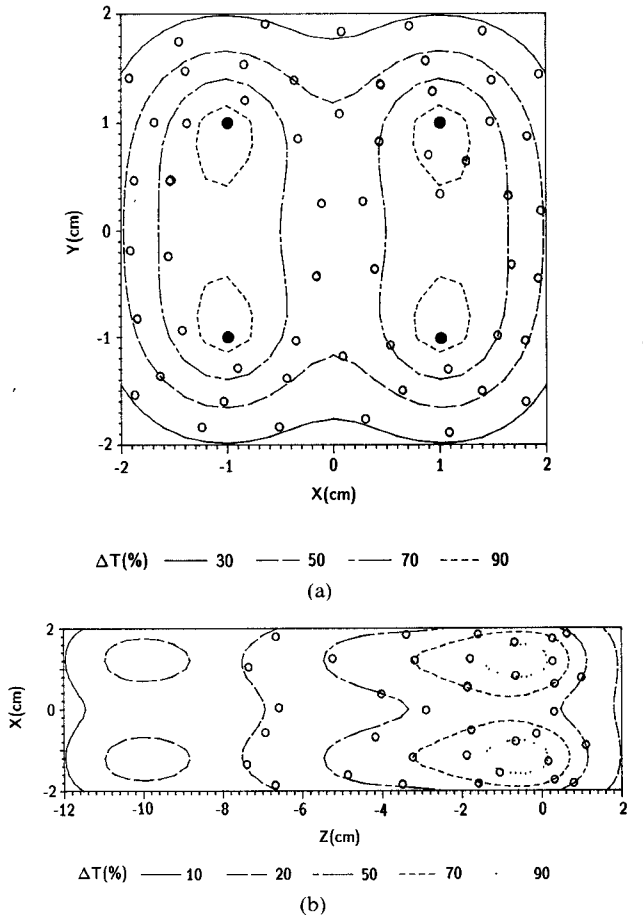

Fig. 5. Theoretical (various contour lines) and measured (open circles) temperature patterns for an antenna array, in which antennas 1 and 4 are in phase at 180°, and antennas 2 and 3 are in phase at 0°. The temperature increments are normalized to their maximum. Labels refer to the normalized isotemperature increment levels in percentage. (a) In the plane $z = 0$, with the antenna positions shown as black dots. (b) Same as (a), but in the plane $y = 0$.

hyperthermia applications. The results shown in Fig. 4 indicate that the four-antenna array, if driven in phase, would heat an ellipsoidal region 6 cm long and 2 cm in diameter. This shape of heating pattern may be desirable for many hyperthermia applications, and reasonably smooth temperature gradients are produced over a fairly large volume.

In Fig. 5, the temperature patterns are shown for an array in which antennas 1 and 4 (on the right in Fig. 5(a)) are in phase at 180°, whereas antennas 2 and 3 (on the left in Fig. 5(a)) are in phase at 0°. Note that the two pairs of antennas are 180° out of phase. In Fig. 5, both the calculated and measured temperature patterns are shown. The isotemperature contours above 70 percent include two separate volumes of 1 cm×2 cm×4 cm around the two antenna pairs respectively. The predicted temperature distributions agree with the measured temperature profiles in both planes. In the axial plane (Fig. 5(b)), the measured temperature pattern does not show a secondary hot spot toward the driven input, even though the theoretical temperature pattern predicts a weak secondary peak at $z = -10$ cm. This difference may occur because the secondary peak is too weak to be measured with our present system. Note that the phase coherence region is no longer at the center of the array, as it was in the case of the in-phase array in Fig. 4. This means that a more uniform temperature distribution in a volume of 2 cm×2 cm×6 cm could be achieved by proper antenna phasing with these sequential time segments: (1) drive the antennas in phase for a given amount of time, (2) drive antennas 1 and 4 in phase at 180° and antennas 2 and 3 at 0°, and (3) drive antennas 1 and 2 in phase at 180° and antennas 3 and 4 at 0°. This phase-modulation technique would appear to generate a more uniform temperature distribution within the entire heated volume, and yield a uniform temperature profile necessary for some hyperthermia applications.

It has been reported that a more uniform power deposition pattern is desirable for raising the temperature to the therapeutic level, while the power deposition pattern with elevated power at the periphery of the tumor is more suitable for maintaining steady-state heating [30], [31]. This type of ideal power deposition can be achieved with the application of the results in Fig. 5. One can eliminate the *SAR* peak at the array center and generate local *SAR* maxima around the array boundary if one chooses the heating sequences (2) and (3) as described in the last paragraph. More research will no doubt yield the optimum phase combinations for generating heating patterns of various desired shapes.

VI. Conclusion

The theory of the insulated asymmetric dipole antenna embedded in a dissipative dielectric medium has been applied to interstitial antenna arrays for microwave-induced hyperthermia applications. The power deposition was computed within the volume of a parallel array of four antennas forming a 2 cm square. The *SAR* calculations of various phase combinations were performed in both lateral ($z = 0$) and axial ($y = 0$) planes, and the effect of coupling between the antennas was neglected. An electric network simulation of heat flow within the volume was developed to convert the *SAR* pattern into the temperature distribution. Comparison of the computed temperature patterns (obtained from the *SAR* distribution through the electrical network analogy) with the experimental measurements has shown an excellent agreement, lending support to the validity of the theoretical analysis. Although the heat conduction system simulated by the electric network in this paper is relatively simple, the technique of the circuit simulation of heat conduction could be applied to a more complicated system. For instance, to simulate heat flow in a biological system, the characteristics of nonlinear blood flow and radiative heat loss are easily incorporated by adding nonlinear convective and radiative elements to the electric network.

Both the theoretical and the experimental results of the present study show that the hottest spot, or the phase coherence region, can be shifted in the lateral plane. Therefore, more uniform *SAR* and temperature distribu-

tions in an extended volume could be achieved if the phase-modulation technique were used. A heating pattern of this type generated by the interstitial antenna array may be ideal for certain clinical hyperthermia applications. If nonuniform heating is desired, it is possible to direct the hot spot to the desired region by properly choosing the driving phase to each antenna.

ACKNOWLEDGMENT

The authors wish to express their appreciation to Dr. R. J. Spiegel for his help on the electrical network simulation and to W. D. Palmer for his help with preparing some of the figures in the paper.

REFERENCES

[1] F. A. Gibbs, M. D. Sapozink, K. S. Gates, and J. R. Stewart, "Regional hyperthermia with an annular phased array in experimental treatment of cancer: Report of work in progress with a technical emphasis," *IEEE Trans. Biomed. Eng.*, vol. BME-31, pp. 115–119, 1984.

[2] J. W. Strohbehn and E. B. Douple, "Hyperthermia and cancer therapy: A review of biomedical engineering contributions and challenges," *IEEE Trans. Biomed. Eng.*, vol. BME-32, pp. 779–787, 1984.

[3] J. Mendecki *et al.*, "Microwave applicators for localized hyperthermia treatment of malignant tumors," *J. Bioeng.*, vol. 1, pp. 511–518, 1977.

[4] L. S. Taylor, "Devices for microwave hyperthermia," in *Cancer Therapy by Hyperthermia and Radiation*, C. Streffer *et al.*, Eds. Baltimore, MD: Urban and Schwarzenberg, 1978, pp. 115–17.

[5] J. W. Strohbehn, E. D. Bowers, J. E. Walsh, and E. B. Douple, "An invasive microwave antenna for locally-induced hyperthermia for cancer therapy," *J. Microwave Power*, vol. 14, pp. 339–350, 1979.

[6] B. E. Lyons, R. H. Britt, and J. W. Strohbehn, "Localized hyperthermia in the treatment of malignant brain tumors using an interstitial microwave antenna array," *IEEE Trans. Biomed. Eng.*, vol. BME-31, pp. 53–62, Jan. 1984.

[7] T. Z. Wong, J. W. Strohbehn, K. M. Jones, J. A. Mechling, and B. S. Trembly, "*SAR* patterns from an interstitial microwave antenna-array hyperthermia system," *IEEE Trans. Microwave Theory Tech.*, vol. MTT-34, pp. 560–567, May 1986.

[8] B. Emami, J. Marks, C. Perez, G. Nussbaum, and L. Leybovich, in *Hyperthermic Oncology*, J. Overgaard, Ed. London: Taylor & Francis, 1984, p. 583.

[9] M. Salcman and G. M. Samaras, "Interstitial microwave hyperthermia for brain tumors," J. Neuro-Oncology, no. 1, pp. 225–236, 1983.

[10] L. S. Taylor, "Electromagnetic syringe," *IEEE Trans. Biomed. Eng.*, vol. BME-25, pp. 303–304, May 1978.

[11] L. S. Taylor, "Implantable radiators for cancer therapy," *Proc. IEEE*, vol. 68, pp. 142–149, Jan. 1980.

[12] K. W. Chan *et al.*, "Changes in heating patterns of interstitial microwave antenna arrays at different insertion depths," *Int. J. Hyperthermia*, vol. 5, no. 4, pp. 499–507, 1989.

[13] R. W. P. King, B. S. Trembly, and J. W. Strohbehn, "The electromagnetic field of an insulated antenna in a conducting or dielectric medium," *IEEE Trans. Microwave Theory Tech.*, vol. MTT-31, pp. 574–583, July 1983.

[14] B. S. Trembly, "The effects of driving frequency and antenna length on power deposition within a microwave antenna array used for hyperthermia," *IEEE Trans. Biomed. Eng.*, vol. BME-32, pp. 152–157, Feb. 1985.

[15] B. S. Trembly *et al.*, "Control of the *SAR* pattern within an interstitial microwave array through variation of antenna driving phase," *IEEE Trans. Microwave Theory Tech.*, vol. MTT-34, pp. 568–571, May 1986.

[16] B. S. Trembly, A. H. Wilson, J. M. Havard, K. Sabatakakis, and J. W. Strohbehn, "Comparison of power deposition by in-phase 433 MHz and phase-modulated 915 MHz interstitial antenna array hyperthermia systems," *IEEE Trans. Microwave Theory Tech.*, vol. 36, pp. 908–916, May 1988.

[17] Y. Zhang, N. V. Dubal, R. Takemoto-Hambleton, and W. T. Joines, "The determination of the electromagnetic field and *SAR* pattern of an interstitial applicator in a dissipative dielectric medium," *IEEE Trans. Microwave Theory Tech.*, vol. 36, pp. 1438–1444, Oct. 1988.

[18] J. P. Holman, *Heat Transfer*, 3rd ed. New York: McGraw-Hill, 1972, ch. 4.

[19] R. J. Spiegel and M. B. E. Fatmi, "A three-dimensional finite-difference thermoregulatory model of a squirrel monkey," *Int. J. Radiat. Oncol. Biol. Phys.*, vol. 12, no. 6, pp. 983–992, June 1986.

[20] H. Jasik, *Antenna Engineering Handbook*. New York, McGraw-Hill, 1961, ch. 3, p. 3-2.

[21] R. W. P. King, R. B. Mack, and S. S. Sandler, *Array of Cylindrical Dipoles*. Cambridge University Press, 1968, ch. 2.

[22] T. T. Wu, R. W. P. King, and D. V. Giri, "The insulated dipole antenna in a relatively dense medium," *Radio Sci.*, vol. 8, no. 7, pp. 699–709, July 1973.

[23] M. Abramowitz and A. Stegun, *Handbook of Mathematical Functions*. Washington, DC: National Bureau of Standards, AMS 55, U.S. Dept. of Commerce, 1964, pp. 916–919.

[24] W. M. McKeeman, "Adaptive numerical integration by Simpson's rule," *Comm. Ass. Comput. Mach.*, vol. 5, Dec. 1962.

[25] W. M. McKeeman and L. Tester, "Nonrecursive adaptive integration," *Comm. Ass. Comput. Mach.*, vol. 6, June 1963, p. 315.

[26] C. K. Chou, G. W. Chen, A. W. Guy, and K. H. Luk, "Formulas for preparing phantom muscle tissue at various radio frequencies," *Bioelectromagnetics*, vol. 5, no. 4, pp. 435–441, 1984.

[27] V. Vladimirescu, K. Zhang, A. R. Newton, D. O. Pederson, and A. Sangiovanni-Vincentelli, *SPICE Version 2G.5.0 User's Guide*, Dept. of Elec. Eng. and Comp. Sci., U. of Calif, Berkeley, CA 94720, June 1982.

[28] *Reference Data for Radio Engineers*, Howard W. Sams & Co., Inc., Indianapolis, IN, 46268, 1975, p. 4–28.

[29] H. S. Ho, A. W. Guy, R. A. Sigelmann, and J. F. Lehmann, "Microwave heating of simulated human limbs by aperture sources," *IEEE Trans. Microwave Theory Tech.*, vol. MTT-19, pp. 224–231, Feb. 1971.

[30] K. B. Ocheltree and L. A. Frizzell, "Determination of power deposition patterns for localized hyperthermia: A steady-state analysis," *Int. J. Hyperthermia*, vol. 3, no. 3, pp. 269–279, 1987.

[31] K. B. Ocheltree and L. A. Frizzell, "Determination of power deposition patterns for localized hyperthermia: A transient analysis," *Int. J. Hyperthermia*, vol. 4, no. 3, pp. 281–296, 1988.

Yang Zhang was born in Shenyang, China, on December 5, 1957. He received the B.S.E.E. degree (with high honors) from the Chengdu Institute of Radio Engineering, Chengdu, China, in 1982, and the M.S. degree in electrical engineering from Duke University, Durham, NC, in 1984. He is presently with the Department of Electrical Engineering, Duke University, as a Research Assistant, where he is working towards the Ph.D. degree in microwave engineering. His research interests are in the area of electromagnetic wave interactions with materials, with applications to transmission lines, antennas, and microwave-induced hyperthermia.

Mr. Zhang is a member of Eta Kappa Nu and Sigma Xi.

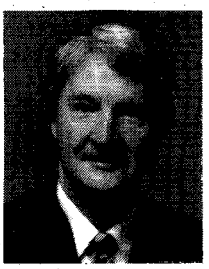

William T. Joines (M'61) was born in Granite Falls, NC, on November 20, 1931. He received the B.S.E.E. degree (with high honors) from North Carolina State University, Raleigh, in 1959, and the M.S. and Ph.D. degrees in electrical engineering from Duke University, Durham, NC, in 1961 and 1964, respectively.

From 1959 to 1966, he was a member of the Technical Staff at Bell Laboratories, Winston–Salem, NC, where he was engaged in research and development work on microwave components and systems for military applications. He joined the faculty of Duke University in 1966, and is currently a Professor of Electrical Engineering. His research and teaching interests are in the area of electromagnetic wave interactions with materials.

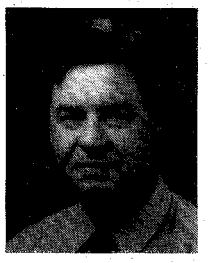

James R. Oleson was born in South Dakota in 1940. He received the Ph.D. degree in physics from the Johns Hopkins University in 1968, specializing in nuclear physics, and the M.D. degree from the University of Arizona in 1976.

From 1968 to 1973 he was a Research Associate with Wesleyan University, Middletown, CT, involved in experimental general relativity and design of an astrometric telescope. Following completion of a Residency in Radiation Oncology in 1979, he was a faculty member in Radiation Oncology at the University of Arizona. Since 1984 he has been at Duke University and is currently a Professor in Radiation Oncology and Principal Investigator of an NCI/NIH Program Project involving the study of hyperthermia in cancer therapy.